Spin Quantum Computing

2

Philipp R. Struck and Guido Burkard

Contents

Abstract

This chapter describes the use of electron spins in semiconductor quantum dots as quantum bits for quantum information processing. Among the central themes of the chapter is the mechanism for a two-qubit operation based on the exchange interaction. Another important topic pertains to the mechanisms that lead to the loss of quantum coherence and are related to phonons or nuclear spins in the host semiconductor. The last part of this chapter is focused on the prospects for extending the ideas of spin-based quantum information to new materials such as graphene, where both nuclear-spin- and phonon-induced decoherence and relaxation are suppressed.

P.R. Struck (✉) • G. Burkard
Department of Physics, University of Konstanz, Konstanz, Germany
e-mail: philipp.struck@conti.de; guido.burkard@uni-konstanz.de

Y. Xu et al. (eds.), *Handbook of Spintronics*,
DOI 10.1007/978-94-007-6892-5_5

List of Abbreviations

13C	Carbon-13
2D	Two dimensional
2DEG	Two-dimensional electron gas
AlGaAs	Aluminum gallium arsenide
As	Arsenic
CNOT	Controlled NOT (NOT is not acronym)
EPC	Electron phonon coupling
Ga	Gallium
GaAs	Gallium arsenide
HF	Hyperfine
InGaAs	Indium gallium arsenide
MoS_2	Molybdenum disulfide
QD	Quantum dot
QPC	Quantum point contact
RSA	Rivest–Shamir–Adleman
SiGe	Silicon–germanium
SO	Spin orbit
SU(2)	Special unitary group in two dimensions
WS_2	Tungsten disulfide
XOR	Exclusive OR (OR is not an acronym)

Introduction

The purpose of this chapter is to provide an introduction and up-to-date overview of spin-based quantum information processing (This chapter is adapted from Struck [1]). We begin with an introduction to quantum computation where we discuss the main requirements which any quantum computer will have to fulfill. Then we show how spins in semiconductor quantum dots can be used to implement quantum information processing and how pairs of spins in adjacent quantum dots can be coupled to each other via the exchange interaction. The standard implementation of spin-based quantum information processing requires single-spin rotations in addition to exchange, but we will explore how quantum computation can be performed with the exchange interaction only. This provides a possible solution for the problem of relatively time consuming and technically challenging single-spin rotations. In the following chapters, we will then shift focus to actual implementations of quantum bits (qubits) and their properties. In particular, we give an overview of the important problem of decoherence, i.e., the loss of quantum information stored in a qubit. We will see that there are two types of information-destroying processes. First we will discuss the relaxation of spins into an energetically lower state. For spins in semiconductor quantum dots, this process is mainly caused by the spin–orbit interaction combined with the spontaneous emission of acoustic phonons. The other process is the loss of coherence of a quantum mechanical superposition caused by nuclear spins in the host material of the quantum dot.

Although the atomic hyperfine interaction is in some sense weaker than the spin–orbit interaction, we will see that in the case of quantum dots, it is in fact the hyperfine interaction that limits the decoherence time. In the penultimate chapter, we discuss qubits based not on a single spin 1/2 but on the singlet and triplet states of two spins 1/2 located in a double-quantum dot which are also the subject of current scientific investigations. In the last chapter of this introduction, we will discuss spin qubits in graphene quantum dots. Up to now, their experimental implementation remains challenging, but the theory predicts long decoherence times due to weak spin–orbit and hyperfine interaction.

Quantum Computation in a Nutshell

Before we turn to the physical implementation of quantum computing devices, let us take a moment to review the reasons why it is of interest to employ the laws of quantum mechanics for computational (more generally, information processing) tasks. While quantum computers cannot outperform classical computers in terms of *which* problems can be solved (*computability*), there is strong evidence that they beat classical computers in terms of *how fast* they can solve certain problems. The first statement means that every task a quantum computer can perform can *in principle* also be done by a (classical) Turing machine and therefore any available computer today. This is understandable as the quantum machine obeys the rules of quantum mechanics as we know them and those rules and equations can be formulated in the language of mathematics which in turn can be formulated as a (classical) computer program. However, computability in itself is typically not the main issue in real-world applications. What is much more important is the efficiency of a computation which can be expressed mathematically in terms of the *complexity* of the problem. As we will see, there are problems which require a time exponentially long in the size n of the input (instance of the problem) when being solved on a classical computer or $\mathcal{O}(e^{cn})$ or more generally, $\mathcal{O}(e^{cn^{\gamma}})$ with $c > 0$ and $\gamma > 0$. This makes those problems intractable *in practice* for classical computers.

What a quantum computer can do is to solve some of these problems much faster than a classical computer. By "much faster," one typically means a speedup from exponential to polynomial complexity, $\mathcal{O}(n^{\alpha})$ with some (hopefully not too large) fixed exponent α. Note however that this is not a general feature of quantum computers. There is no theorem which states that there is a more efficient quantum version of any given classical algorithm. However, so far, there exist a number of quantum algorithms which are much more efficient than their known classical counterparts. One of the most striking examples of a quantum speedup is the algorithm proposed by Peter Shor to find the prime factors of a given integer number [2]. Public-key cryptography schemes such as RSA rely on the fact that the factorization of sufficiently large numbers is practically impossible with classical computers.

Before we start the discussion of specific implementation of qubits and quantum gates using spins in solid state, it is instructive to think about the general

requirements for a working and useful quantum computer. David DiVincenzo proposed five criteria which any system which is a candidate for a quantum computer must fulfill [3] and which we briefly review in the following:

1. Many qubits are required for a working quantum computer. Hence we have to demand scalability, i.e., the possibility to combine an arbitrary number of qubits to form larger registers needed to store and process information. Solid-state qubits are very promising in this respect because they can be manufactured using conventional semiconductor fabrication techniques. The scalability requirement mathematically translates to that of a *precisely enumerable* Hilbert space. This sensible requirement means that we have to know the exact number of qubits in which we want to use to store and to manipulate information. Furthermore, it should be possible to decompose the Hilbert space into a direct product of the individual qubit Hilbert spaces. As a result, the dimension of the total Hilbert space grows exponentially, and for 10 qubits, i.e., 10 two-level systems, it is already $2^{10} = 1{,}024$-dimensional. In principle, one can use systems with more than two levels to do quantum computing, but in the following, we will always refer to two-level systems (*qubits*).
2. In order to actually start a quantum computation, it is necessary to initialize the system, i.e., prepare the entire qubit register into a known and well-defined state such as "all qubits 'zero.'" This is easily done in some systems by simply cooling the qubits to their ground states. However, if one uses nuclear spins, this criterion turns out to be harder than it sounds, and one may need to resort to active (dynamical) cooling schemes.

   Besides the obvious necessity to initialize the qubits, supplying the system with low-entropy states is also important in the context of quantum error correction where it is a means of extracting entropy from the system which builds up due to (unavoidable) decoherence [4].
3. The relevant decoherence times of the qubits must be longer than the gate operation times. This requirement at first sounds most challenging for solid-state systems such as the spin qubits we are discussing here. Unlike, e.g., trapped atoms hovering in vacuum, the electron spin in a solid interacts with a rather noisy environment. Memoryless decoherence processes of a single qubit can be described using two time constants: the so-called energy relaxation time T_1 and the decoherence time T_2.

   The T_2 time describes how long it takes until a coherent quantum superposition of $|0\rangle$ and $|1\rangle$ described by the pure qubit state $|\psi\rangle = \alpha|0\rangle + \beta|1\rangle$ turns into an incoherent mixture of $|0\rangle$ and $|1\rangle$ described by the density matrix $\rho = |\alpha|^2|0\rangle\langle 0| + |\beta|^2|1\rangle\langle 1|$, where α and β are complex numbers. In some of the most important semiconductor materials such as GaAs, the dominant cause for the loss of phase coherence of electron spin qubits is the hyperfine interaction with the surrounding nuclear spins (although this environment is typically not memoryless). The nuclear-spin-induced decoherence can be avoided to a large extent by the use of materials with few or no nuclear spins such as carbon, silicon, or germanium.

Spin qubits in graphene will be discussed in more detail in section "Spin Qubits in Graphene." The mechanisms leading to energy relaxation in spin qubits will be discussed in section "Spin Relaxation in Quantum Dots."

In order to perform quantum computations, the typical time T_{op} required to perform an elementary one- or two-qubit operation must be much smaller than the decoherence time. Another way of stating this requirement is to say that the error probability per gate needs to be small, $\varepsilon = T_{\mathrm{op}}/T_2 \ll 1$. The same condition must be fulfilled for the relaxation time T_1, but in most cases $T_1 \gtrsim T_2$ as we will see in section "Nuclear-Spin-Induced Decoherence." The fact that in practice $\varepsilon > 0$ forces us to find ways of coping with the errors that occur during a quantum computation. This is an interesting and nontrivial issue which deserves a detailed treatment which we cannot give in this chapter. For a good introduction to quantum error correction, we refer the reader to the available textbooks [4–6]. Let us merely remark that under certain assumptions regarding the nature of the errors, fault-tolerant quantum computation has been proven to be possible when the error rate per gate ε lies below a certain threshold $\varepsilon_{\mathrm{th}}$. The value of the threshold depends on the details of the type of errors as well as on the type of quantum error correction used. Typical values for standard quantum error correction schemes are $\varepsilon_{\mathrm{th}} \approx 10^{-4}$, but recently, methods to achieve a higher threshold have not been reported [7, 8].

4. The fourth criterion provides the link between the hardware and the software: a universal set of quantum logic gates needs to be implemented. A quantum logic gate, or just *quantum gate* for short, is simply a unitary operation U on a finite number of qubits (one or two qubits in the following). A quantum algorithm can be understood as a series of quantum gates $U_k U_{k-1} \ldots U_2 U_1$ acting on the qubits that form the memory of the computer.

   Generally speaking, the unitary operator describing the quantum gate is obtained as

$$U = T\exp\left(-\frac{i}{\hbar}\int_0^t H(t')\,dt'\right) \tag{1}$$

   where $H(t)$ describes the time-dependent control Hamiltonian of the system and T is the time-ordering operator. The exact form of the Hamiltonian depends on the system under consideration and can involve externally applied magnetic or electric fields. Formally, finding a Hamiltonian H to perform a desired gate operation U as in Eq. 1 is straightforward. However, this may lead to unphysical interactions and therefore the physical implementation can still be challenging, including many-body interactions or strong magnetic fields.

   The set of quantum gates to be implemented needs to be *universal*, i.e., any unitary operation on an arbitrary number of qubits needs to have a (finite) decomposition into a product of unitaries from this set. It is known [9] that a universal set can be made from all (unitary) one-qubit operations $U \in SU(2)$, which can be identified with spin rotations, in combination with one appropriate two-qubit operation $U_{(2)}$ (This came somehow as a surprise in the early days of

quantum computing because in *reversible* classical computing three-bit gates are necessary to form a universal set), i.e.,

$$S = \{U_{(2)}\} \cup SU(2). \tag{2}$$

One popular choice for the two-qubit operator $U_{(2)}$ is the CNOT gate, which is the quantum version of the XOR gate [10]. CNOT is short for *controlled* NOT and it is one instance of the general set of two-qubit gates in which the state of one qubit, say, the first one, acts as a control parameter of an operation performed on the second qubit, the so-called *target* qubit. In this case, the second qubit is flipped if the first qubit is in the state $|1\rangle_1$, where $|i\rangle_j$ with $i, j = 0,1$ denotes the basis states. If the control qubit is in the state $|0\rangle_1$, the gate acts as an identity operator, i.e., nothing happens. The effect of the CNOT gate on all four basis states is the following:

$$|0,0\rangle \mapsto |0,0\rangle, \tag{3}$$

$$|0,1\rangle \mapsto |0,1\rangle, \tag{4}$$

$$|1,0\rangle \mapsto |1,1\rangle, \tag{5}$$

$$|1,1\rangle \mapsto |1,0\rangle. \tag{6}$$

In this basis, it is easy to write down the matrix representation of the gate as

$$\mathbf{U}_{\text{CNOT}} = \begin{pmatrix} 1 & 0 & 0 & 0 \\ 0 & 1 & 0 & 0 \\ 0 & 0 & 0 & 1 \\ 0 & 0 & 1 & 0 \end{pmatrix}. \tag{7}$$

We would like to stress at this point once more the difference between classical and quantum bits. For the former, the CNOT gate is nothing but an XOR gate where the target bit is the result of the addition modulo 2. In the quantum case, the input and output states can be much more intricate. For example, consider the effect of a control state in a superposition $|\psi\rangle_1 = \frac{1}{\sqrt{2}}\left(|0\rangle_1 + |1\rangle_1\right)$ on a target state $|\psi\rangle_2 = |0\rangle_2$. The initial state can be written as a product state

$$|\psi\rangle_1 \otimes |\psi\rangle_2 = \frac{1}{\sqrt{2}}|0\rangle \ \ (|0\rangle + |1\rangle). \tag{8}$$

The final state is easily calculated as

$$\mathbf{U}_{\text{CNOT}}\left(|\psi\rangle_1 \otimes |\psi\rangle_2\right) = \frac{1}{\sqrt{2}}(|0\rangle \ \ |0\rangle + |1\rangle \ \ |1\rangle), \tag{9}$$

which cannot be written as a product state anymore. We have created an entangled state which is impossible with classical bits. As an alternative to the

CNOT gate, the square-root-of-SWAP gate together with one-qubit rotation also forms a universal set of quantum gates [11]. We will come back to this gate in the section on universal quantum computing with exchange interactions.

5. After the computation, individual qubits have to be measured. In the case where the measurement takes place in the computational basis given by $|0\rangle$ and $|1\rangle$, the associated observable to be measured is the Pauli operator

$$\sigma_z = \begin{pmatrix} 1 & 0 \\ 0 & -1 \end{pmatrix}. \tag{10}$$

After this description of the requirements that a system has to meet in order to be useful for quantum computations, we now give an example of a quantum algorithm that could run on such a machine. We will introduce the Deutsch algorithm as an instructive example and refer the reader to Nielsen and Chuang [4] and Mermin [6] for a thorough introduction to quantum computation. The piece of quantum software with most practical relevance known so far is arguably Shor's algorithm for efficiently factoring large integer numbers [2]. Perhaps even more relevant are the prospects of efficiently simulating quantum systems with a quantum computer, which typically turns out to be very hard when using conventional computers [12].

Let us introduce the notation for the description of quantum computational processes. A quantum gate acting on states of n qubits is described by a unitary transformation $\mathbf{U}$ which can be represented as a unitary $2^n \times 2^n$ matrix (conventionally also denoted by $\mathbf{U}$). In the simplest case of single-qubit operations, $\mathbf{U}$ is a 2×2 matrix. Unitaries necessarily describe reversible functions, but we can also use them to compute arbitrary functions f by retaining the input state $|x\rangle$ together with the output state $|y\rangle$ as $|x\rangle\ |y\rangle$ and write the transformations as matrices acting on both states. The unitary transformation acting on the two states can be written as

$$U_f|x\rangle\,|y\rangle = |x\rangle|y \oplus f(x)\rangle \tag{11}$$

where $\oplus$ denotes the XOR operation ($0 \oplus 0 = 1 \oplus 1 = 0, 1 \oplus 0 = 0 \oplus 1 = 1$) or bitwise addition modulo 2. If the output register is set to zero at the beginning, we find

$$U_f|x\rangle\,|0\rangle = |x\rangle\,|f(x)\rangle, \tag{12}$$

and therefore the output state contains the desired function of the input state.

As an instructive example, let us now turn to the Deutsch algorithm [13] whose task is to determine whether a given function $f(x) : \{0,1\} \to \{0,1\}$ is balanced ($f(0) \neq f(1)$) or constant ($f(0) = f(1)$). One can think about this task in terms of classical objects. This illustration is not just useful for the purpose of making things more understandable, but it also highlights the point that although the actual computation of a quantum computer follows the laws of quantum mechanics, the input and output are typically classical. Let's suppose we have a coin and want to

find out whether it is biased or not, i.e., whether it shows head or tail on both sides or not. The easiest way is to look on one side, turn the coin, and compare the outcome to the other side. So one needs two elementary operations (here, observations of one side of the coin), or two evaluations of the function $f(x)$, to find an answer. And obviously two is also the minimum number of evaluations or operations that suffices to complete the task.

Deutsch showed that by means of quantum mechanics, it is possible to do the same in one single step. (In the original algorithm, this is possible only with a success rate of 1/2. Later it was shown that is also possible to get an answer in a single step every time.) The basic idea is to use a superposition of both states as an input state, let the algorithm operate on this superposition of both possible inputs, and then do the readout. A superposition of basis states is often required in quantum computing and it is therefore instructive to learn about the quantum gate that does the job. The gate is called the Hadamard gate (after the French mathematician Jacques Salomon Hadamard (1865–1963)) and has the form

$$H = \frac{1}{\sqrt{2}}(\sigma_x + \sigma_z) = \frac{1}{\sqrt{2}}\begin{pmatrix} 1 & 1 \\ 1 & -1 \end{pmatrix}. \tag{13}$$

If we let H act on one of the two basis states, we obtain the superpositions

$$H|0\rangle = \frac{1}{\sqrt{2}}(|0\rangle + |1\rangle), \quad H|1\rangle = \frac{1}{\sqrt{2}}(|0\rangle - |1\rangle). \tag{14}$$

To solve the problem, Deutsch suggested to use an initial state which contains all possible combinations of input and output states at the same time, i.e., as a superposition. As just shown, this state can be made by using Hadamard gates

$$|\psi\rangle = H \otimes H|0\rangle|1\rangle = \frac{1}{2}(|0\rangle + |1\rangle)\ \ (|0\rangle - |1\rangle). \tag{15}$$

The unknown function U_f is now applied to this state. Following Eq. 12 and making use of $|0 \oplus f(x)\rangle = |f(x)\rangle$ and $|1 \oplus f(x)\rangle = \sigma_x|f(x)\rangle$, where σ_x is the single-qubit NOT operation, one obtains

$$U_f|\psi\rangle = (-1)^{f(0)}\Big[|0\rangle + (-1)^{f(1)-f(0)}|1\rangle\Big](|0\rangle - |1\rangle) \tag{16}$$

A measurement in the $|0\rangle \pm |1\rangle$ basis (equivalent to a Hadamard and a σ_z measurement) in the first register yields the desired information, whether f is constant or balanced. This would not have been possible with *any* classical computer or algorithm. The key feature of quantum mechanics that has been used to obtain this result is sometimes called *quantum parallelism*. Note, however, that we could not have obtained both values of f at once, because this information cannot be extracted from the final state (a global phase cannot be measured). So, the output state contains exactly what we wanted to know, and not a bit more (literally!).

The Loss–DiVincenzo Proposal

In their proposal for electron spin-based quantum information processing, Loss and DiVincenzo showed how a universal set of one- and two-qubit gates can be implemented on a register of coupled spin qubits located in an array of quantum dots [11]. As will be shown in detail below, the entangling two-qubit unitary gate $U_{(2)}$ directly emerging from the exchange interaction between spins in adjacent quantum dots is the square-root-of-SWAP gate. A combination of square-root-of-SWAP gates and single-spin rotations can then also produce the more standard CNOT gate. Single-spin rotations generated by some local magnetic interaction form the set $SU(2)$ which completes the universal set of gates. As described above, this combined set of gates is universal in the sense that they can be combined in a quantum circuit, i.e., a sequential application of quantum gates, to perform arbitrary quantum algorithms. There exist other variants of this proposal that rely on the same type of exchange interactions, e.g., involving the nuclear or electron spins of donor atoms buried in a silicon substrate [14], or electron spins in SiGe quantum dots [15], or electrons trapped by surface acoustic waves [16]. For a recent review of spin-based quantum computing systems, see Kloeffel and Loss [17] (Fig. 1).

One can model such spin qubits in a quantum dot array using the well-known Hubbard model in which the tunnel hopping strengths t_{ij} are pulsed, i.e., are functions of time t. High tunnel barriers effectively switch the coupling between neighboring qubits i and j off with exponential precision ($t_{ij} = 0$), while for a coupling parameter much smaller than the onsite Coulomb repulsion (charging) energy U, i.e., $t_{ij} \ll U$, the description can be restricted to the charge sector with one electron per dot (half-filling of the Hubbard model). The spins experience a Heisenberg coupling

$$H(t) = \sum_{\langle ij \rangle} J_{ij}(t)\, \mathbf{S}_i \cdot \mathbf{S}_j, \tag{17}$$

with a time-dependent exchange coupling $J_{ij}(t) = 4t_{ij}^2(t)/U$. The microscopic origin of the exchange coupling lies in the fact that the energy of the spin singlet is lowered by J due to virtual hopping processes, while the spin triplet remains unaffected because hopping is forbidden by the Pauli exclusion principle. The value of the exchange coupling in dependence of external fields and the inter-dot distance can be obtained from a Heitler–London or Hund–Mulliken ansatz [19]. We can identify the projection operator onto the spin singlet state formed by the spins on sites i and j as $P_{ij}^S = \left|S_{ij}\right\rangle \left\langle S_{ij}\right| = 1/4 - \mathbf{S}_i \cdot \mathbf{S}_j$ and rewrite the Hamiltonian as

$$H(t) = -\sum_{\langle ij \rangle} J_{ij}(t)\, P_{ij}^S = \sum_{\langle ij \rangle} H_{ij}(t), \tag{18}$$

where $H_{ij}(t) = -J_{ij\rightarrow}(t) P_{ij}^S$ and where a (time-dependent) term proportional to the identity has been omitted since it only produces an irrelevant global phase.

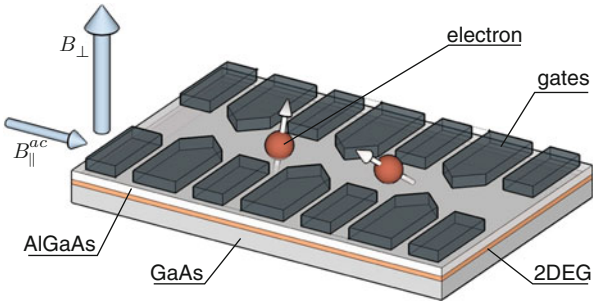

Fig. 1 Schematic of a lateral spin quantum dot array with one excess electron per dot. The spin of the electron on each quantum dot represents a qubit [11]. Indicated here are only two adjacent spins while a quantum register would consist of a large array of qubits. Such a quantum dot array can be realized in various semiconductor heterostructures such as GaAs. The free electrons caused by the doping form a two-dimensional electron gas (2DEG) of typically ≈10 nm thickness at the interface of the heterostructures which is located 50–100 nm below the surface [18]. Regions of confinement can be created by applying voltages to the metallic gates on *top* (as shown) or on the *bottom* of the heterostructure. A constant magnetic field is used to induce a Zeeman splitting; varying magnetic and electric fields may be used to manipulate the spins. The Heisenberg exchange interaction can be employed to couple spins in adjacent quantum dots. The size of such a device is approximately on the order of 100–1,000 nm

Making use of the projector identity $\left(P_{ij}^S\right)^2 = P_{ij}^S$, we can easily find the time evolution operator for coupling two specific qubits i and j (while all other couplings are set to zero) by exponentiating the Hamiltonian. We obtain

$$U_{ij}(\phi) = e^{-\frac{i}{\hbar}\int_0^t dt' H_{ij}} = 1 + \left(e^{i\phi} - 1\right)P_{ij}^S, \tag{19}$$

where

$$\phi = \hbar^{-1}\int_0^t dt' J_{ij}(t'). \tag{20}$$

A π-pulse of the exchange interaction, defined as

$$\phi = \frac{1}{\hbar}\int dt J_{ij}(t) = \pi \mod 2\pi\,, \tag{21}$$

will implement a SWAP gate,

$$\mathrm{SWAP}_{ij} = U_{ij}(\pi) = 1 - 2P_{ij}^S, \tag{22}$$

which precisely interchanges the states of the qubits i and j. While the SWAP gate by itself is not useful for quantum computation, it can be used to shuttle around

qubits and thus to overcome the locality of the exchange interaction in situations where distant qubits need to be coupled. Therefore, while the Hamiltonian (17) solely couples neighboring qubits directly, a series of SWAP gates, which exchange the states in two neighboring qubits, in principle allows for operations between two arbitrary qubits can be accomplished. As we will see in section "Universal Quantum Computing with the Spin Exchange Coupling," there are also proposals how to couple distant qubits and thus avoiding the extra time required for a series of SWAP operations.

To implement a useful entangling gate for universal quantum computation, one can pulse the interaction such that

$$\phi = \frac{1}{\hbar}\int dt J_{ij}(t) = \pm\frac{\pi}{2} \mod 2\pi\,. \tag{23}$$

Such a pulse generates a square-root-of-SWAP gate (up to an irrelevant global phase factor). The square-root-of-SWAP gate has been implemented experimentally in a double-quantum dot [20]. With Eq. 23, the square-roots-of-SWAP gates $S_\pm$ are obtained as (the other two square roots are obtained by changing the overall sign of the unitary)

$$S_{ij}^{\pm} = U_{ij}(\pm\pi/2) = 1 + (\pm i - 1)P_{ij}^{S} = \frac{1 \pm i}{2} + \frac{1 \mp i}{2}\mathrm{SWAP}_{ij}. \tag{24}$$

Let us pick the positive sign and omit the fixed indices i and j in what follows. The gate $S = S^+$ together with single-qubit rotations is just as universal as the abovementioned CNOT gate. In fact, together with single-spin rotations $U_i(\phi) = \exp(i\phi\mathbf{S}_i)$ about axis i with an angle ϕ, the square-root-of-SWAP gates can be converted into a *controlled phase-flip* gate [11]

$$U_{\mathrm{CPF}} = e^{i\pi/2}e^{-i\pi S_1^z/2}e^{i\pi S_2^z/2}Se^{-i\pi S_1^z}S \tag{25}$$

which in turn is equal to the CNOT gate up to a basis change. In the presence of spin–orbit coupling, the exchange coupling Eq. 17 can acquire anisotropic terms which do not conserve S_z [21]. However, it turns out that in the first order, it is possible to eliminate these terms by using time-symmetric gate pulses [22].

So far, we have discussed how a number of spin qubits coupled via the exchange interaction can be used to construct a universal set of quantum gates which is a necessary requirement for a working quantum computer. As we have learned in section "Quantum Computation in a Nutshell," another requirement is that the gate operation time is much shorter than the decoherence time of the spins involved. But in any case, there will be some amount of decoherence during a gate operation. In addition to the proposal described above, in Loss and DiVincenzo [11], the nonideal situation of a SWAP operation during which the spins are coupled to a magnetic environment is studied using a (quantum) master equation.

Universal Quantum Computing with the Spin Exchange Coupling

In the previous section, we discussed how the exchange interaction between two qubits can be used to implement a universal set of quantum gates. The relative strength, short range, and large on-off ratio of the Heisenberg exchange coupling allow for fast gate operations. For the operation of spin-1/2 qubits, in addition to the Heisenberg coupling Eq. 17, one needs single-spin operations generated by some form of local magnetic field, giving rise to a Hamiltonian,

$$H(t) = \sum_{\langle i,j \rangle} J_{i,j}(t) \mathbf{S}_i \cdot \mathbf{S}_j + \mu_B \sum_i g_i(t) \mathbf{B}(\mathbf{r}_i, t) \cdot \mathbf{S}_i = H_{\mathrm{ex}}(t) + H_Z(t), \tag{26}$$

where H_Z is the local Zeeman term necessary for the single-spin rotations.

We are now going to address to question whether the exchange coupling alone might be sufficient for universal quantum computation. The straightforward answer to this question for spin-1/2 qubits is "no," because the Heisenberg interaction preserves both the total angular momentum and the magnetic quantum number

$$\left[H_{ex}, S^2\right] = \left[H_{ex}, S_z\right] = 0 \tag{27}$$

which immediately means that without supply of additional single-qubit operations, it cannot be universal, because it cannot explore the entire computational Hilbert space. This means that when one starts with a state having a certain sharp value of, say, total S_z as an input of the computation, then only states with that same value of S_z could result from the time evolution under the exchange interaction. However, for universal quantum computing, every final state would have to be reachable in principle, since this might be demanded by the quantum algorithm.

There are practical motivations to do without the single-spin rotations. The control over individual spins located very close to each other makes single-qubit rotations quite challenging. It requires the local (de)tuning of the Zeeman splitting $g\mu_B B$ away from resonance, so that Rabi oscillations are suppressed. The standard way to rotate spins is by electron spin resonance (ESR), i.e., using a small oscillatory magnetic field perpendicular to a larger static magnetic field. Applying rf magnetic-field pulses locally, on a scale of 10–100 nm, without inducing photon-assisted tunneling, in order to achieve single-spin ESR, however, requires advanced techniques [23]. The gradient in the static magnetic field required for selective ESR on one of the dots only can be induced by the surrounding nuclear spins [23] or alternatively by a micromagnet [24].

The requirement for single-spin rotations can be circumvented if instead of a single spin 1/2 as the qubit representation, one makes use of multiple spins 1/2 which remain in a two-dimensional subspace of the Hilbert space with fixed total spin quantum numbers. The smallest number of spins 1/2 that allows for an encoding for which the Heisenberg interaction alone is universal is three [25]. (Note that the general scheme of quantum computing using only the exchange coupling is not only restricted to quantum dots using electronic spins but can be

applied to other systems described by isotropic exchange coupling.) In this case, two of the spins form either a singlet ($S = 0$) or triplet ($S = 1$). Together with the third spin, the total spin of the three qubits is either $S = 1/2$ or $S = 3/2$. One can choose, for example, the two states with $S = 1/2$ and $S_z = 1/2$ as the computational basis. The Heisenberg interaction conserves these quantum numbers and does not cause transitions non-computational states. An explicit choice for the basis states of the encoded qubit could be [25]

$$|0\rangle = |S\rangle|\uparrow\rangle = \frac{1}{\sqrt{2}}(|\uparrow\downarrow\rangle - |\downarrow\uparrow\rangle)\,|\uparrow\rangle \tag{28}$$

$$\begin{aligned} |1\rangle &= \sqrt{\frac{2}{3}}|T_+\rangle|\downarrow\rangle - \sqrt{\frac{1}{3}}|T_0\rangle|\uparrow\rangle \\ &= \sqrt{\frac{2}{3}}|\uparrow\uparrow\rangle|\downarrow\rangle - \sqrt{\frac{1}{6}}(|\uparrow\downarrow\rangle + |\downarrow\uparrow\rangle)|\uparrow\rangle. \end{aligned} \tag{29}$$

The state $|0\rangle$ can be prepared by applying a sufficiently strong magnetic field to align the third spin, i.e., $g\mu_B B > k_B T$, but sufficiently small in order not to destroy the singlet, i.e., $g\mu_B B < J_{ij}$.

The important question remains: what is the computational overhead one has to accept, i.e., how many more operations are necessary to do implement a chosen set of universal gates? The implementation of a two-qubit gate with three spins encoding each qubit means one in principle has to deal with a Hilbert space of dimension $2^{2\cdot 3} = 64$. The question of how much overhead the use of encoded qubits produces can be reformulated by asking how can one produce a two-qubit gate on the encoded qubits which is *equivalent* to a CNOT gate or, more quantitatively, how many two-spin exchange interactions, so-called *pulses*, are necessary to produce a two-qubit gate which is equivalent to a CNOT gate. A sequence of 19 pulses was found numerically [25] and it was later confirmed analytically that this sequence indeed produces a CNOT gate [26]. It should be mentioned, however, that this only works if the qubits are in a specific subspace of the computational subspace. It takes additional steps to produce this necessary initial state. Sequences which do not have this requirement have been found with a length of 23 pulses [27] and 39 pulses [28]. Recently, there has been renewed interest in three-spin encoded qubits where the exchange coupling is left on and is supplemented by radio-frequency pulses [29–31].

There are other ways how the exchange interaction can be used to implement quantum gates. If a locally changing g-factor can be engineered, e.g., by an appropriate choice of the material surrounding a qubit, it is sufficient to use pairs of spins to implement logical qubits. In this case, the computational overhead is reduced as only two gate operations are needed for a controlled π-phase flip [32]. Instead of using a locally varying g-factor, one can also use the anisotropic XY interaction on a set of spins to construct encoded qubits. The advantage is again a smaller number of gate operations in comparison to the Heisenberg exchange-only proposal [33]. Single- and two-qubit gates can be implemented for even more general exchange Hamiltonians [34].

Optimization of Quantum Circuits

If several of the interactions in Eq. 26, i.e., exchange and local magnetic fields, can be controlled simultaneously and independently, then the CNOT gate (or, equivalently, the controlled phase-flip gates) can be implemented without using the sequence Eq. 25 in a single parallel interaction pulse. In the case of identical pulse profiles for the two magnetic fields, a CNOT between qubits 1 and 2 can be achieved with the magnetic field applied in z-direction with pulse strengths [35]

$$B_1 = \frac{1+\sqrt{3}}{2} \frac{J_{12}}{g\mu_B}, \tag{30}$$

$$B_2 = \frac{1-\sqrt{3}}{2} \frac{J_{12}}{g\mu_B}, \tag{31}$$

where the magnitude of the inter-dot exchange coupling pulse J_{12} determines the gate time $T_{\text{gate}} \sim \hbar/J_{12}$. In general, more complicated operations can be optimized by breaking up the time evolution into discrete steps with constant parameters J_{ij} and $B_{\alpha,i}$ where $\alpha = x, y, z$.

Spin Relaxation in Quantum Dots

Up to now, we have considered perfect qubits which maintain their quantum mechanical state as long as they are not operated on or read out. In reality, this is never exactly the case. In fact, decoherence is one of the biggest challenges in building a usable quantum computer. However, the third DiVincenzo criterion (see section "The Loss–DiVincenzo Proposal") only requires that the decoherence has to be maintained much longer than the gate operation time and not infinitely long. How much longer depends on the details of how errors during a quantum computation are corrected (quantum error correction is an interesting subject of its own which we will not discuss here). To fulfill the above requirement, two things can be done. First, the gate operations should be performed as fast as possible, and second, a system has to be chosen which exhibits only weak decoherence. Spin qubits typically have much longer decoherence times compared to charge qubits.

Before we go into the details of spin relaxation processes, we need to clarify what we mean by *relaxation* and *decoherence*. So far, we have used the term "decoherence" to describe any process which destroys or alters the qubit states in a noncontrollable way both during and in between gate operations. However, to be precise, there are two distinct ways this can happen for qubits (Fig. 2). Decoherence in its strict meaning refers to a transition of a coherent superposition of states, e.g., of the $|0\rangle$ and $|1\rangle$ of the qubit, into a statistical mixture of these states (this process is sometimes also referred to as pure decoherence or dephasing). *Spin relaxation*, on the other hand, describes essentially the decay of the higher-energy qubit state (say, $|1\rangle$) into the lower-energy one ($|0\rangle$ in our example). If the qubit is coupled to an

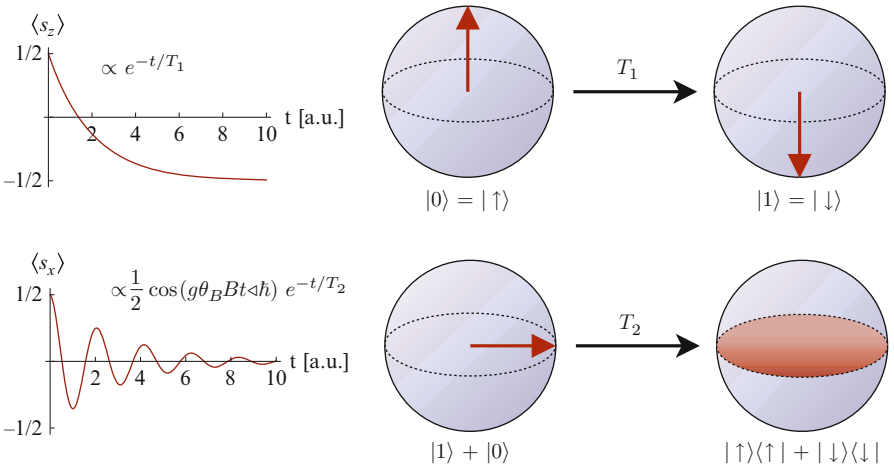

Fig. 2 This figure illustrates the two processes which lead to loss of information of a qubit. On the right-hand side, Bloch spheres are used to illustrate the spin states in a QD. The states $|\uparrow\rangle$ and $|\downarrow\rangle$ are eigenstates of σ_z that are separated in energy by an external magnetic field along the z-direction. The *upper row* depicts a spin relaxation process in which a spin prepared in an σ_z eigenstate flips due to exchange of energy with the environment. It is characterized by an exponential decay with relaxation time T_1. The *lower row* illustrates the decoherence which describes the decay of quantum mechanical superpositions in to statistical mixtures when the system initially is in an eigenstate of, e.g., σ_x. The time scale for this process is given by the decoherence time T_2. Note that T_2 describes the decay of a single system during a single run of the experiment. An experimentally more useful measure is the dephasing time T_2^* which arises from averaging over an ensemble of nuclear-spin configurations. It is often considerably shorter than T_2

environment with a temperature comparable with the qubit energy splitting (divided by k_B), then there can be random excitations in the reverse direction and the qubit relaxes to a thermal equilibrium. In the case of Markovian noise (i.e., short correlation times of the environment of the spin qubit), these two processes are described by exponential decays with time constant T_1 for spin relaxation and T_2 for decoherence. If the latter is in addition averaged over many samples or many experimental runs, then one conventionally uses the notation T_2^* for the inhomogeneous decoherence time.

Spin relaxation refers to the process of a flipping of $|\uparrow\rangle$ to $|\downarrow\rangle$. This decay is typically caused by the emission of a phonon carrying the Zeeman energy away into the bulk crystal lattice. The correlation time of the phonon bath is very short, and thus the spin–phonon interaction is Markovian to a good approximation and, hence, spin relaxation is usually exponential. On the other hand, decoherence, as was already mentioned, is the transition of a coherent transverse state, such as an σ_x eigenstate $|\uparrow\rangle + |\downarrow\rangle$, in the presence of a magnetic field along z, into an incoherent mixture $|\uparrow\rangle\langle\uparrow| + |\downarrow\rangle|\uparrow\rangle$. This decay can be exponential as well but for the case of the nuclear-spin bath, it is typically more complicated as we will see in section "Nuclear-Spin-Induced Decoherence."

For the remainder of this section, we will be dealing with spin relaxation. The host material for many experiments with single-electron spins in quantum dots is the two-dimensional electron gas (2DEG) formed at the interface between layers of GaAs and AlGaAs. The dominating mechanism for spin relaxation in QDs in which a pair of Zeeman sublevels of the lowest orbital state is used as a qubit can be described using the Hamiltonian [36] $H = H_0 + g\mu_B B S_z + H_{\mathrm{SO}} + H_{\mathrm{EPC}}$ where $H_0 = p^2/2m + U(\mathbf{r})$ and the exact form of the confining potential U only has a minor influence on the relaxation time. The eigenenergies of $H_0 + g\mu_B B S_z$ can be written as $E_n \pm \frac{1}{2} g\mu_B B$, where the sign in front of the Zeeman energy corresponds to the two-spin eigenstates $\sigma = \uparrow = +1$ and $\sigma = \downarrow = -1$. In the absence of structural inversion symmetry in the crystal hosting the 2DEG, a spin–orbit interaction of the Rashba type is present, $H_{\mathrm{SO}} = \Delta_R(-\sigma_x p_y + \sigma_y p_x)$ [37]. As a consequence, the Zeeman sublevels which form the qubit are not product states of up- and downspin with one orbital level anymore. Instead, each sublevel n acquires a small admixture of different orbital states m and opposite spin. The amount of this admixture is given by the ratio of the spin–orbit coupling Δ_R and the single-particle level spacing, and due to the smallness of this parameter, the problem of finding the new eigenstates can be treated perturbatively,

$$|n\sigma\rangle = |n\sigma\rangle^{(0)} + \sum_{m\neq n} \frac{{}^{(0)}\langle m, -\sigma|H_{\mathrm{SO}}|n\sigma\rangle^{(0)}}{E_n - E_m \mp \frac{1}{2} g\mu_B B} |m, \alpha\rangle^{(0)}, \tag{32}$$

where $|n\sigma\rangle$ denotes the spin–orbit admixed states and $|m\sigma\rangle^{(0)}$ the unperturbed eigenstates of $H_0 + g\mu_B B S_z$. These new eigenstates are still orthogonal (to lowest order), but the electron–phonon coupling H_{EPC} enables transitions between them. The transition matrix elements are given as

$$\langle \mathbf{q}|\langle n\sigma|H_{\mathrm{EPC}}|n, -\sigma\rangle|0\rangle = \sum_{m\neq n} \left(\frac{(H_{\mathrm{EPC}})^{\mathbf{q}}_{mn} (H_{\mathrm{SO}})^{\uparrow\downarrow}_{nm}}{E_n - E_m - g\mu_B B} + \frac{(H_{\mathrm{SO}})^{\uparrow\downarrow}_{nm} (H_{\mathrm{EPC}})^{\mathbf{q}}_{nm}}{E_n - E_m + g\mu_B B} \right) \tag{33}$$

The processes related to this matrix element can be described as a spin flip accompanied by a transition to an energetically higher level due to the spin–orbit interaction H_{SO}, followed by a decay back to the lower orbital via the emission of a phonon with wave vector $\mathbf{q}$. Here, $|0\rangle$ and $|\mathbf{q}\rangle$ denote the phonon vacuum and the state with a single phonon with wave vector $\mathbf{q}$, respectively (here, we assume that the temperature of the phonon bath is much smaller than the Zeeman splitting $g\mu_B B$). In a second possible process, the electron–phonon coupling acts first and then the spin–orbit coupling.

With the above equation, the spin relaxation rate can be calculated by using Fermi's Golden Rule,

$$\frac{1}{T_1} = 2\pi A_{\mathrm{dot}} \int \frac{\mathrm{d}^d q}{(2\pi)^d} |\langle \mathbf{q}|\langle n\downarrow|H_{\mathrm{EPC}}|n\uparrow\rangle|0\rangle|^2 \delta\left(\epsilon_{\mathbf{q}} - g\mu_B B\right), \tag{34}$$

with the dot area A_{dot} and the phonon dispersion $\epsilon_{\mathbf{q}}$ and wave vector $\mathbf{q}$. Depending on the dimensionality of the material, the phonons can move in $d = 3$ (GaAs), $d = 2$ (graphene), or $d = 1$ (carbon nanotubes) dimensions. For acoustic phonons, $\epsilon_{\mathbf{q}} = sq$ with the sound velocity s.

In the case of a single-valley direct-bandgap semiconductor such as GaAs, the bound-state Zeeman sublevels $|n\sigma\rangle$ and $|n,-\sigma\rangle$ occurring in Eq. 33 are time-reversed partners of each other, i.e., at vanishing magnetic field $B = 0$, they form a degenerate Kramers pair. As a consequence, the matrix element Eq. 33 vanishes in the limit $B = 0$. Formally, the two terms of Eq. 33 cancel because the electron–phonon matrix element is symmetric with respect to the exchange of its indices, while the spin–orbit matrix element is antisymmetric. This so-called Van Vleck cancelation [38] reduces the matrix element at small values of B by a factor $\propto B$ and thus the relaxation rate by a factor of B^2. The energy dependence of the density of states of 3D acoustic phonons $\rho \propto q^2 \propto \epsilon_q^2 \propto B^2$ combined with the q-dependence of the matrix elements $\propto q^{1/2} \propto B^{1/2}$ lead to $T_1 \propto B^{-5}$ for low fields [36] which was confirmed experimentally [39]. At sufficiently low fields, the spin relaxation time was found to exceed 1 s. The cancelation can be traced back to the time-reversal invariance of H and its eigenstates at $B = 0$, i.e., the fact that both spin–orbit interaction and electron–phonon coupling preserve time-reversal symmetry. Note that this is the case in GaAs and many other semiconductors but there are cases where time-reversal symmetry can be broken by a specific choice of states for the qubit. In the case where one picks two states of opposite spin from one of the two K-valleys in graphene as a qubit, then these states are not time-reversed partners and thus Van Vleck cancelation does not occur (see section "Spin Qubits in Graphene").

Instead of electrons, the spins of holes confined to quantum dots can also be used as qubits. While the spin relaxation time T_1 depends very strongly on the applied B-field [40], relaxation times of more than 0.2 ms have been measured for self-assembled heavy-hole quantum dots in InGaAs [41, 42].

Nuclear-Spin-Induced Decoherence

Energy relaxation of the electron spin in a quantum dot on the order of $T_1 \approx 1$ s has been observed [39] which means that these processes can be slower than the typical gate operation times T_{op} by many orders of magnitude, since $T_{\mathrm{op}} \approx 100$ ns (single-qubit operations) and $T_{\mathrm{op}} \lesssim 1$ ns (two-qubit operations). However, we also require $T_2 \ll T_{\mathrm{op}}$ and it turns out that in GaAs T_2 is much shorter than T_1 due to the coupling of the electron spin to the surrounding nuclear spins. The ensemble-averaged coherence time T_2^* is typically around 10 ns in electrostatically defined GaAs QDs. Before we turn to the description of nuclear-spin-induced electron spin decoherence, we point out that the spin–orbit coupling which is responsible for T_1 also has an effect on T_2 which is much weaker than the effect of the nuclear spins in GaAs and in the absence of nuclear spins would lead to a T_2 on the same order as T_1. To see this, we consider the following argument due to Golovach et al. [43].

In the case of a laterally confined electron with single-particle level spacing $\hbar\omega_0$ and the presence of both Dresselhaus-type (intrinsic) and Rashba-type (extrinsic) spin–orbit interaction, an effective Hamiltonian is obtained by means of a Schrieffer–Wolff transformation,

$$H_{\text{eff}} = g\mu_B(\mathbf{B} + \delta\mathbf{B}(t)) \cdot \mathbf{S}, \tag{35}$$

which corresponds to the coupling of the electron spin $\mathbf{S}$ to an effective fluctuating time-dependent magnetic field $\delta\mathbf{B}(t)$ caused by the phonons. Interestingly, these fluctuations are always transverse to the applied field, i.e., $\delta\mathbf{B} \perp \mathbf{B}$. Using the Bloch equations to calculate the relaxation and dephasing times, one finds that for the case of purely transverse B-field fluctuations $\delta\mathbf{B}$ the relation $T_2 = 2T_1$ holds. In the special case of equally strong intrinsic and extrinsic spin–orbit interactions, the relaxation rate $1/T_1$ approaches zero in lowest order in the electron–phonon coupling and in all orders of the spin–orbit coupling. In this limit, other processes such as direct spin–phonon coupling and dephasing via two-phonon processes become important.

Since in fact $T_2^* \ll T_1$ in GaAs QDs, there must be another mechanism leading to fast spin decoherence, i.e., a short T_2^*. There is a large body of evidence leading to the conclusion that the dominant decoherence mechanism for the electron spin in GaAs QDs is the hyperfine interaction with the roughly $10^5 - 10^6$ nuclear spins of the Ga and As atoms surrounding the electron. Although the hyperfine interaction is relatively weak, the large number of nuclear spins can lead to a sizable fluctuation in the effective nuclear magnetic field (Overhauser field) which leads to fast electron spin decoherence.

To obtain an understanding of how the hyperfine interaction causes decoherence, we first consider its microscopic origin (see, e.g., Coish [44] and Coish and Baugh [45]). To start with, there is the atomic hyperfine interaction between a spinful nucleus and a single electron. There are two ways how to derive a Hamiltonian. A nonrelativistic derivation starts from a hydrogen atom with an additional vector potential $\mathbf{A} = \frac{\mu_0}{4\pi}\frac{\mathbf{M}\times\mathbf{r}}{r^3}$ with $\mathbf{M}$ as the magnetic dipole moment of the atomic nucleus and μ_0 the permeability of free space. The vector potential $\mathbf{A}$ enters the Hamiltonian via minimal coupling and in the form of an additional term which couples the electron's spin to the magnetic field $\mathbf{B} = \nabla \times \mathbf{A}$. After making use of Gauss' law and taking the limit of the radius of the proton being zero, one arrives at the hyperfine Hamiltonian which has three contributions:

- A coupling between the nuclear spin $\mathbf{I}$ and the electron's orbital angular momentum $\mathbf{L}$ of the form $H_{\text{HF}}^{L} \propto \mathbf{I} \cdot \mathbf{L}$, which resembles the (regular) spin–orbit interaction
- A dipole-type spin–spin interaction between the nuclear and electron spins which consists of two terms, $H_{\text{HF}}^{\text{dip},1} \propto \frac{\mathbf{I}\cdot\mathbf{S}}{r^3}$ and $H_{\text{HF}}^{\text{dip},2} \propto \frac{(\mathbf{I}\cdot\mathbf{r})(\mathbf{S}\cdot\mathbf{r})}{r^5}$, where $\mathbf{r}$ denotes the distance vector between the electron and the nucleus
- A contact interaction $H_{\text{HF}}^{\text{c}} \propto \mathbf{I} \cdot \mathbf{S}\delta(\mathbf{r})$

A more elegant derivation starts from the relativistic Dirac equation in the presence of the same vector potential **A** as above. The equation can be rewritten into an eigenvalue problem for the electron part of the four-component spinor. Taking the nonrelativistic limit $E \ll mc^2$, one obtains the same terms of the hyperfine interaction. In addition, this derivation also gives rise to the spin–orbit interaction as we have seen in a previous section "Spin Relaxation in Quantum Dots."

An electron (or hole) in a quantum dot is not bound to a single atomic nucleus, as it would be in an atom, but is loosely bound and is in contact with the spins of about 10^4–10^6 atomic nuclei. Of the three types of hyperfine interaction mentioned, not all contribute equally to decoherence. When the electron's wave function is of *s*-type symmetry, the contact interaction $H_{\mathrm{HF}}^{\mathrm{c}} \propto \mathbf{I} \cdot \mathbf{S}\delta(\mathbf{r})$ is dominant. The other terms decay strongly with the distance r like $H_{\mathrm{HF}}^{\mathrm{L}} \propto r^{-3}$. The hyperfine interaction between a single-electron spin **S** and a large number of nuclear spins $\mathbf{I}_k$ in a QD is obtained by summing over all atomic nuclei,

$$H_{\mathrm{HF}} = \sum_k A_k \mathbf{I}_k \cdot \mathbf{S} = g\mu_B \mathbf{B}_n \cdot \mathbf{S}, \tag{36}$$

where the coupling constants A_k depend on the electron wave function at the position $\mathbf{r}_k$ of the k-th nucleus, $A_k \propto |\psi(\mathbf{r}_k)|$. In Eq. 36, we have defined the Overhauser field $\mathbf{B}_n = \sum_k A_k \mathbf{I}_k / g\mu_B$ which describes the effective magnetic field seen by the electron due to the nuclear spins. For the case of a fully polarized nuclear-spin bath in the QD, the absolute value of the magnetic field can be quite large. For example, in GaAs where $A \approx 90\ \mu$eV and $I = 3/2$, one finds $B_n^{\max} \approx 5$T [45]. In equilibrium, however, the nuclear spins will be far from being polarized. Only a very small number of spins will be aligned along the external B-field. The distribution of the polarization in thermal equilibrium is given by a Boltzmann distribution with fluctuation around B_n given by $\approx B_n^{\max}/\sqrt{N}$ which amounts to a value of a few mT for a number of nuclear spins $N \approx 10^4$–10^6 [45]. These random fluctuations are the key to decoherence. The effects of the static fluctuations of the nuclear spins lead to a reduction of the inhomogeneous decoherence time T_2^* but this effect can be undone using spin-echo techniques. However, there are also time-dependent fluctuations of $\mathbf{B}_n = \sum_k A_k \mathbf{I}_k$, coming from two different microscopic origins and leading to a reduction of T_2 which cannot be undone with spin echo. The first source of those fluctuations is the internuclear magnetic dipole–dipole interaction which causes flip-flop processes where two nuclei simultaneously flip (or change) their spin. At sufficiently large external field, these processes conserve total nuclear spin, but even then the flip–flip event typically takes place between nuclei with different values of A_k such that the value of the Overhauser field is changed. If the nuclear spin is larger than 1/2, there are typically inhomogeneous quadrupolar splittings which suppress nuclear-spin diffusion and can lead to a prolongation of the electron spin coherence [46]. The second source of temporal nuclear field fluctuations is the hyperfine interaction between the electron and the nuclei itself [47].

Just as the spin–orbit interaction, the hyperfine interaction can cause both spin dephasing and spin relaxation. However, whereas the spin–orbit interaction dominates the relaxation time T_1, the hyperfine interaction mainly limits the dephasing time T_2. By rewriting Eq. 36 as

$$H_{\mathrm{HF}} = \sum_k A_k \mathbf{I}_k \cdot \mathbf{S} = \frac{1}{2} \sum_k A_k \left(I_k^+ S^+ + I_k^- S^- + 2 I_k^z S^z \right), \tag{37}$$

with $I^{\pm}$ the nuclear spin and $S^{\pm}$ the electron spin raising and lowering operators, we see that spin flips are caused by the transverse components $B_n^{x,y}$ of the nuclear field assuming the external magnetic field $\mathbf{B}_0$ to be along the z-direction. However, typically $B_n^{x,y} \ll B_0$ and thus the energy transfer is very small compared to the level distances of the electron in the QD. Thus the contribution of this process to the spin relaxation time T_1 is small.

Spin relaxation can also occur in a nuclear-spin–orbit-type interaction. $B_n^{x,y}$ depends on the orbital symmetry of the electron's wave function via the coupling constants A_k. They in turn depend on the overlap of the wave function with the nuclei. In effect, the spin and orbital degree of freedom are mixed, and in analogy to the case of "actual" spin–orbit interaction, relaxation is possible via the emission of a phonon. While this effect is typically weak, it is the limiting factor for the spin relaxation time T_1 at very low magnetic fields.

The main contribution of the hyperfine interaction to decoherence is the dephasing caused by fluctuations in both amplitude and phase of the longitudinal component of the Overhauser field B_n^z. These random fluctuations yield the electron spin a random phase over the time in which it evolves. The exact law of the dephasing depends on the details of the distribution of the nuclear spin. When B_n^z is randomly chosen from a Gaussian distribution, the dephasing would also be of a Gaussian type, i.e., $\propto \exp\left[-t^2/\left(T_2^*\right)^2\right]$. For typical fluctuations of ≈ 1 mT, the resulting dephasing time is on the order of ns [20].

Here, we want to point out that the hyperfine interaction as presented before is in principle similar for electrons and holes. However, the coupling constants are different in the case of holes. Their wave functions have a p-type symmetry and thus vanish at the origin, i.e., at the position of the nucleus. For this reason, the contact hyperfine interaction does not play a role for hole QDs. Instead the anisotropic term and the coupling to the orbital degree of freedom of the electron dominate. A difference exists between light and heavy holes. The coupling of the latter to the nuclear-spin bath takes the form of an Ising interaction $\sum_k A_k I_k^z S_k^z$ instead of the isotropic Heisenberg coupling [48].

Since the surrounding nuclear spins are the main cause for the decoherence of the electron and hole spin in a quantum dot, one has several options toward improving coherence. The first option is to manipulate the nuclear-spin bath in such a way as to minimize nuclear-spin fluctuations and thus electron and hole decoherence. One possible way of achieving this would be to prepare a highly polarized nuclear-spin system [19]. However, to gain a factor of 10 in the spin

decoherence time, a polarization of 99 % would be required [49]. So far, nuclear-spin polarization up to 70 % has been experimentally achieved via dynamical nuclear polarization [50]. However, full nuclear polarization is not necessary to reduce the nuclear field fluctuations; it is sufficient to narrow the nuclear-spin distribution, i.e, to reduce the fluctuation in the Overhauser field. This can in principle be achieved electrically [51, 52] or optically [53, 54]. These methods can lead to improvements in the decoherence times of several orders of magnitude. The second option in response to nuclear-spin-induced decoherence is to use materials with low nuclear-spin density; see section "Spin Qubits in Graphene."

Singlet–Triplet Qubits

In the following, we will discuss qubits encoded in the spin of a pair of electrons in a double-quantum dot (Fig. 3), consisting of two QDs next to each other with a tunable tunnel barrier in between [32, 55, 56]. Each individual dot can be independently loaded with electrons by lowering the energy level of the respective dot with electrostatic gates [18]. We shall focus on charge states of the double-quantum dot with two electrons in total. Using the notation (n,m) where n and m correspond to the electrons in each of the dots, the two-electron configurations of interest are (2, 0), (1, 1), and (0, 2). The states of the two electrons can be categorized according to their total spin, i.e., one singlet state S and three triplet states $T_{0,+,-}$. The triplet states in the configurations (2, 0) and (0, 2) are energetically unfavorable because the Pauli exclusion principle requires one of the electrons to be in an excited state, and hence these two states can be neglected (or, better, they are eliminated via a Schrieffer–Wolff transformation to yield the exchange coupling). The actual qubit is then encoded in the singlet and one of the triplets, e.g.,

$$S = \frac{1}{\sqrt{2}}(|\uparrow\downarrow\rangle - |\downarrow\uparrow\rangle), \quad T_0 = \frac{1}{\sqrt{2}}(|\uparrow\downarrow\rangle + |\downarrow\uparrow\rangle). \tag{38}$$

For the initialization of a qubit, the energy of the first QD is lowered such that only a charge configuration of (2, 0) is favorable. When two electrons are then loaded into the first dot, they will be in a singlet state which is lower in energy than the triplet states. To perform operations, the system is brought adiabatically into the (1, 1) configuration (the adiabaticity is with respect to the tunnel coupling t; in the presence of nuclear spins, the transition actually needs to be non-adiabatic with respect to the hyperfine coupling). Coherent rotations $S \leftrightarrow T_0$ can be performed by magnetic-field gradients which can be created either by dynamic nuclear polarization [51] or micromagnets [24] brought in vicinity of the double QD. Reading out the spin state can be accomplished by spin-to-charge conversion. This works similarly to the initialization. The energy of the first dot is lowered again. When the qubit in the (1, 1) configuration is in a singlet state $S(1, 1)$, a transition to $S(2, 0)$ is energetically favorable. However, when the qubit is in a state $T_0(1, 1)$, the Pauli

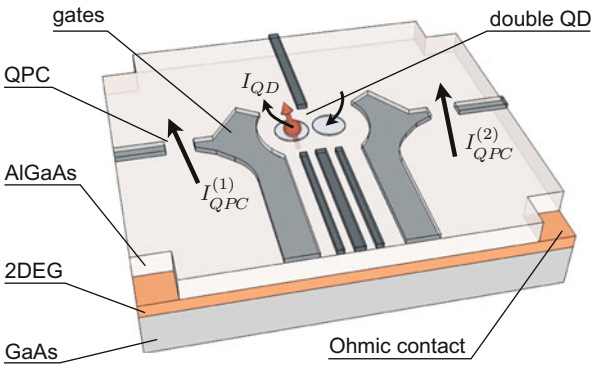

Fig. 3 An illustration of a typical GaAs double-quantum dot. The coupling of the two dots in the center of the device can be tuned by the two long gates in the center. For the readout of the spin states, a spin-to-charge conversion based on Pauli spin blockade is used. The two quantum point contacts (QPCs) on both sides sense how many electrons, i.e., 0, 1 or 2, are in each quantum dot. The current is measured at the Ohmic contacts at the corner of the device

principle implies that the configuration $T_0(2, 0)$ requires one of the electrons to occupy a higher orbital level which is energetically unfavorable. Thus, when measuring the charge in the first QD, only one electron will be detected if the state was a spin triplet. The required charge readout can be performed by quantum point contacts (QPCs) as shown in Fig. 3. The conductance of a QPC is quantized and when it is tuned very close to a transition between two conductance plateaus, very small changes in the charge of a capacitively coupled device lead to measurable changes in current through the QPC [18].

Using double QDs has several advantages over single QDs. One advantage of singlet–triplet qubits is their controllability with electric fields [56]. Moreover, the decoherence time T_2 can be up to 500 times longer which corresponds to $\approx 280\ \mu$s. On top of that, double QDs allow for faster operation times τ_{op} and thus allow more operations to be performed before coherence is lost. Up to $T_2/\tau_{\text{op}} \approx 9 \times 10^3$ operations are possible for a double QD versus ≈ 22 for a single QD. A good overview of state-of-the-art performance numbers can be found in Ref. 21. Additionally, double QDs feature a higher readout fidelity ≥ 90 %. The price to be paid for these advantages is the added complexity in building and operating a double dot, as well as a significantly shorter spin relaxation time of $T_1 \approx 5$ ms versus $T_1 > 1$ s in a single dot [39].

Spin Qubits in Graphene

So far, we have considered implementations of quantum dots in "conventional" semiconductors, such as GaAs. These systems are relatively mature and well understood, and the feasibility of all required operations for a quantum computer

has been experimentally demonstrated [18]. As mentioned before, spin relaxation times of more than one second [39] and decoherence times sufficiently long to allow for 9×10^3 operations [17] have been measured. However, the decoherence caused by the surrounding nuclear spins in the host material remains challenging and adds complexity to those qubits. In the light of its low nuclear-spin density, it seems natural to use carbon-based materials for spin qubits, in particular graphene, the two-dimensional allotrope of elemental carbon [57]. The isotope mixture of naturally occurring carbon is such that it consists of 99 % ^{12}C which has no nuclear spin and only 1 % ^{13}C with nuclear spin 1/2; hence the hyperfine interaction is expected to play only a minor role. Furthermore, spin–orbit interaction in graphene is expected to be relatively weak due to the low atomic mass of carbon and therefore long relaxation times are expected. There are also cases where spin–orbit coupling is desirable for electrically controlled spin manipulation. Bilayer graphene offers the possibility to induce and regulate a Rashba spin–orbit coupling with a perpendicular electric field [58]. The transition metal dichalcogenide family (such as MoS_2, WS_2, etc.) offers two-dimensional semiconductors with a relatively strong spin–orbit coupling and an interesting gapped graphene-like band structure [59] which might be interesting for spintronics [60] and spin qubits.

Aside from all the promising properties, there are some challenges that need to be overcome before graphene can be used for spin-based quantum information processing. First, the gapless linear spectrum prevents the localization of particles in an electrostatic potential well; this phenomenon from relativistic quantum mechanics is called the *Klein paradox*. Second, the valley degeneracy in graphene (as in other group IV elemental solids such as Si and Ge) endows the Heisenberg exchange interaction with additional complexity which needs to be dealt with when performing exchange-based quantum gates [57, 61].

To understand these issues, let us look at the microscopic structure of graphene, a single layer of graphite, or equivalently, a two-dimensional arrangement of carbon atoms in a hexagonal lattice [62]. The carbon atoms in the graphene lattice are bonded via hybridized sp^2 orbitals, i.e., one s orbital and the p_x and p_y orbitals hybridize to three σ orbitals which lie within a plane and form the bonds between the carbon atoms. The electron in the remaining p_z orbital is weakly bound and therefore responsible for the curious peculiar electronic properties of graphene. Another important ingredient is the hexagonal lattice structure (see Fig. 4), consisting of a triangular Bravais lattice with a two-atomic basis. Another way to think about it is as two triangular sublattices (A and B). The reciprocal lattice of graphene is also a hexagonal lattice and at the six corners the conduction and valence bands touch in single points. Only two of these points, denoted by K and K', are different (modulo reciprocal lattice vectors).

A simple but – for many purposes – sufficient theoretical description of the band structure is obtained from a simple tight-binding model. It is assumed that the weakly bound electrons in the p_z orbitals can hop to their nearest neighbors with a hopping matrix element t. Since all three neighboring sites of any given atom are of the contrary

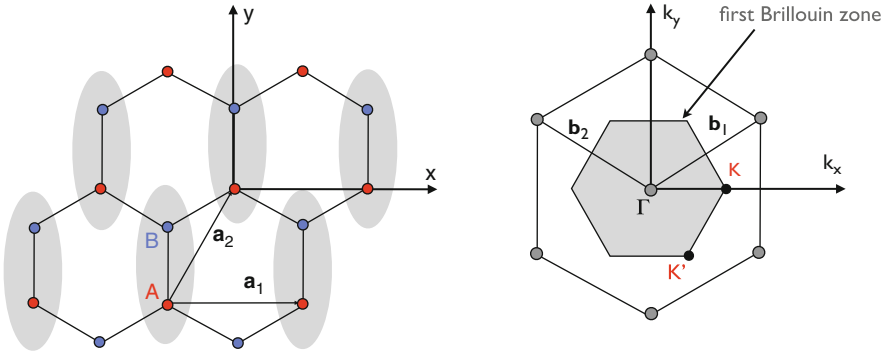

Fig. 4 Graphene is made of a hexagonal lattice of carbon atoms with a bond length of $a/\sqrt{3} = 0.142$ nm where $a = |\mathbf{a}_1| = |\mathbf{a}_2| = 0.246$ nm is the lattice constant. This two-dimensional solid can be described as a trigonal Bravais lattice with a two-atomic basis, or equivalently, as two trigonal sublattices, denoted by A and B. The first Brillouin zone has the same hexagonal symmetry as the lattice in real space. At the six corners, the conduction and valence bands touch in single points, two of which (K and K') are distinct (modulo reciprocal lattice vectors). The regions around K and K' are also referred to as the two valleys of graphene

sublattice type, hopping only occurs between different sublattices to a good approximation. The dispersion relation obtained from the tight-binding model is

$$E(\mathbf{k}) = \pm\gamma\sqrt{1 + 4\cos\frac{\sqrt{3}ak_y}{2}\cos\frac{ak_x}{2} + 4\cos^2\frac{ak_x}{2}} \tag{39}$$

where $a = 2.46 \times 10^{-10}$ m is the lattice constant and $\gamma = 2.8$ eV the nearest-neighbor hopping energy. As can be seen in Fig. 5, the dispersion relation reflects the symmetry of the lattice. To a good approximation around the two K-points, the dispersion relation can be treated as linear in the momentum k,

$$E(\mathbf{k}) = \pm\hbar v_F|\mathbf{k}|, \tag{40}$$

with $v_F = 10^6$ m/s as the Fermi velocity. The charge carriers, i.e., electrons and holes, in graphene behave like ultrarelativistic massless particles. Hence, they can be described by a Dirac–Weyl equation for massless particles,

$$H_0\psi = -i\hbar v_F\boldsymbol{\sigma}\cdot\nabla\psi = E\psi, \tag{41}$$

where $v_F \sim 10^6$ m/s is the Fermi velocity. The vector $\boldsymbol{\sigma}$ consists of the Pauli matrices σ_x and σ_y which act on the pseudo-spin, i.e., on the sublattice space. The free solutions of this equation have the form

$$\psi(x,y) = \begin{pmatrix}\psi_A(x,y)\\ \psi_B(x,y)\end{pmatrix} = e^{ik_x x}e^{ik_y y}\begin{pmatrix}1\\ \pm e^{i\phi}\end{pmatrix}, \tag{42}$$

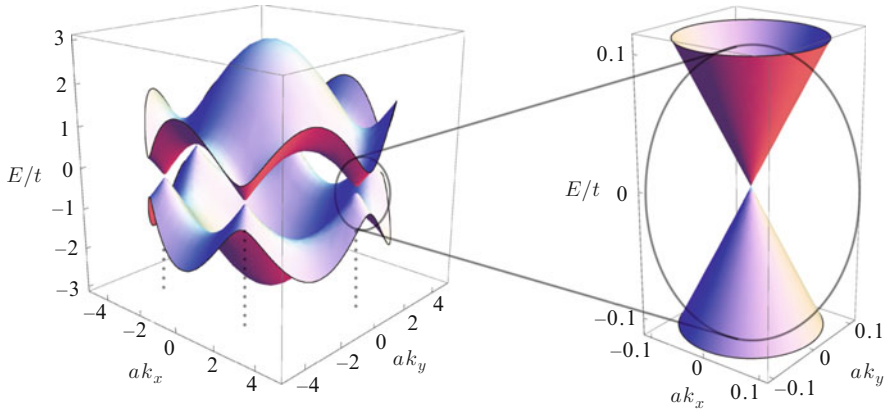

Fig. 5 On the *left*, the band structure of graphene, Eq. 39, as obtained from a tight-binding model including only nearest-neighbor hopping is shown. It reflects the hexagonal symmetry of both the lattice and the reciprocal lattice. The energy is given in units of the next-nearest-neighbor hopping energy $t = 2.8$ eV, $a = 2.46$A. Around each K-point where the conduction and valence bands touch, the band structure can be approximated by linear dispersion $E(k) = \pm\hbar v_F|\mathbf{k}|$ as shown on the right. This approximation is valid for energies $\lesssim 1$ eV. Thus the charge carriers in graphene behave like massless relativistic fermions

with eigenenergies $E = \pm\hbar v_F|\mathbf{k}|$ and $k_x = |\mathbf{k}| \cos\phi$ and $k_y = |\mathbf{k}| \sin\phi$. Again, note the spinor structure of the wave function which is due to the two sublattices. If we now add an additional potential barrier, it is diagonal in the sublattice space, i.e., it does not mix the pseudo-spin.

To find the wave function in the presence of a, say, rectangular barrier, one has to solve the equation in each region separately and put the pieces together at the interfaces. However, because the Dirac equation is a first-order differential equation, only the wave function but not its derivative needs to be matched. The resulting transmission coefficient as a function of the incident angle is plotted for different heights of the potential barrier in Fig. 6. One can see that, irrespective of the barrier heights, electrons arriving at a right angle always pass the barrier as if it wasn't there [62]. This is the Klein paradox.

The reason why we discussed the Klein paradox is that it makes building spin qubits with graphene quantum dots more challenging than it is for "regular" semiconductors. One has to come up with clever ways how to trap and guide charge carriers. In the following, we will present three ways on how to deal with this. In addition to the Klein paradox, there is another issue in graphene which we have briefly mentioned before. The first Brillouin zone has the same structure as the lattice itself and therefore it has two independent K-points. The eigenstates of a free charge carrier are degenerate in this degree of freedom which is not desirable if the aim is to build a pure two-level system which serves as a qubit. In fact, a lifted valley degeneracy is necessary for the spin-only Heisenberg exchange interaction to appear.

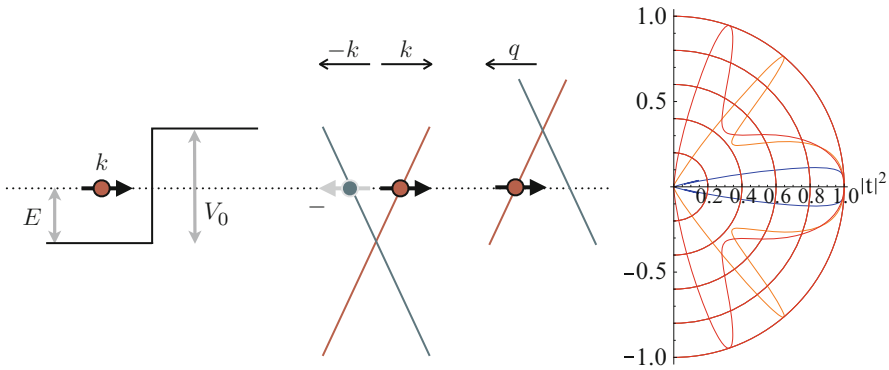

Fig. 6 This figure illustrates the Klein paradox in (gapless) graphene. When an electron with energy E and momentum k impinges on the barrier of height V_0 head-on, it is never scattered back. In the center, the dispersion relations outside (*left*) and inside (*right*) the barrier are shown. The *green* and *red lines* describe the dispersion of the forward moving and backscattered particles, which lie on the respective Dirac cones. The *dotted line* marks the Fermi energy up to which all states are occupied. As the charge carriers are chiral, the pseudo-spin (*black arrow*) is along the direction of the momentum and fixed to one branch of the cone. The electron entering the barrier continues its propagation as a hole or vice versa. On the right-hand side, the transmission $|t|^2$ of an electron with energy $E = 80$ meV through a barrier of thickness 100 nm is shown as a function of the barrier heights 100 meV (*red*), 200 meV (*orange*), and 300 meV (*blue*) are shown

One idea how to circumvent both the Klein paradox and the valley degeneracy problems is to use graphene nanoribbons [57]. For armchair boundaries with alternating A and B atoms along the edge and suitable width, it turns out that such ribbons become one-dimensional semiconductors with a small bandgap $\propto \hbar v_F/W$ [63], in which the valley degeneracy is lifted in the lowest subband [64]. A semiconducting armchair nanoribbon can be used to build a QD using electrostatic gates due to the finite gap [57]. For a width of $W \approx 30$ nm, a gap of ≈ 60 meV is opened, which is a fairly small value compared to conventional semiconductors. As a result, only a small number of confined states can exist in such a graphene nanoribbon quantum dot. The length of the ribbon as well as the back-gate voltage can be used to adjust the number of bound states. A logical extension of a single QD on a graphene ribbon would be an array of QDs next to each other, forming a quantum register. The experimental demonstration of a double-quantum dot in a graphene nanoribbon has been reported [65]. It is an interesting question how to couple such QDs to each other via the Heisenberg exchange coupling which is used to construct a universal set of quantum gates (see section "Universal Quantum Computing with the Spin Exchange Coupling"). Since the valley degeneracy can be lifted in armchair graphene nanoribbons, the exchange coupling will have its usual (spin-only) form in this case. It is even possible to utilize the nearby valence band in order to obtain a nonlocal (quasi-long range) exchange coupling between distant spin qubits [66]. It is challenging to fabricate nanoribbons with well-defined edges. While it is likely that the precise form of the

edge will not matter for the opening of a bandgap, disordered edges tend to give rise to additional bound states at the edge or additional unintended quantum dots which are problematic. It is therefore interesting to consider the alternative of graphene quantum dots without atomic boundaries where a bandgap is opened by breaking the inversion symmetry in graphene, either due to a substrate [67] (e.g., BN) or a perpendicular electric field (in particular, in bilayer graphene).

Here, we briefly discuss the proposal for electrostatically defined quantum dots in gapped single or bilayer graphene [68]. The experimental realization of quantum dots in graphene remains challenging due to the smallness of the gap in many cases. Recently [69], confinement and Coulomb blockade in bilayer graphene sandwiched between boron–nitride dielectrics was reported. To describe bound states in a graphene quantum dot with a circular confinement potential in gapped graphene, one can write separate Hamiltonians for the two valleys [68]

$$H_\tau = v_F(\mathbf{p} + e\mathbf{A}) \cdot \boldsymbol{\sigma} + \tau\Delta\sigma_z + U(\mathbf{r}), \tag{43}$$

where the valley-isotropic form of the Dirac spinors was used and where a magnetic field $\mathbf{B} = \nabla \times \mathbf{A} = (0, 0, B)$ has been introduced. In polar coordinates, one finds the solution wave functions

$$\Psi^\tau(r, \varphi) = e^{i(j-1/2)\varphi} \begin{pmatrix} \chi_A^\tau(r) \\ \chi_B^\tau(r) e^{i\varphi} \end{pmatrix}, \tag{44}$$

with the components

$$\chi_\sigma^\tau(r) = 2^{(1+n_\sigma)/2} e^{-br^2/2} r^{n_\sigma} \times \begin{cases} \alpha_\sigma U(q_\sigma, 1 + n_\sigma, br^2), & r > R, \\ \beta_\sigma M(q_\sigma, 1 + n_\sigma, br^2), & r < R, \end{cases} \tag{45}$$

where U and M denote confluent hypergeometric functions (reducing to Bessel functions in the limit $B = 0$) and where $b = eB/2$, $a_\sigma = 2b(j + \sigma/2) - (\epsilon^2 - \Delta^2)/v^2$. Here, j is the eigenvalue of the total angular momentum $J_z = -i\partial_\varphi + \sigma_z/2$, $n_\sigma = |j - \sigma/2|$ and $q_\sigma \equiv \frac{1}{4}\left[\frac{a_\sigma}{b} + 2(1 + n_\sigma)\right]$. The coefficients α_σ and β_σ are calculated using the continuity condition for the wave function at the circumference of the QD. Interestingly, the valley degeneracy can by lifted with the magnetic field (Fig. 7).

Spin Relaxation in Graphene

Spin relaxation in graphene can be expected to be quite different from that in GaAs (section "Spin Relaxation in Quantum Dots") because:

1. In contrast to spin sublevels in a direct-bandgap valley-nondegenerate semiconductor, in graphene the qubit states obtained from two opposite spins and the same orbital state in a given valley do not form a Kramers pair because time-reversal maps one valley to the other. Hence, there is no Van Vleck cancelation.

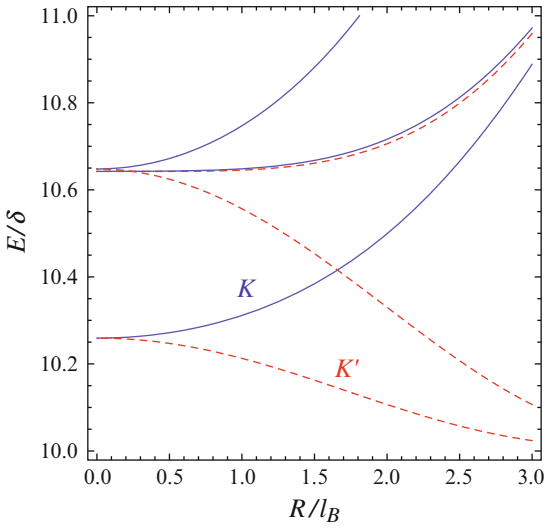

Fig. 7 Lowest conduction band energy levels in a circular quantum dot in gapped graphene. The QD has radius R and is obtained by electrical gating. The magnetic field B leads to a splitting of the states into two valleys of graphene [68] (here, $l_B = \sqrt{\hbar/eB}$ denotes the magnetic length). Energies are plotted in units of $\delta = \hbar v_F/R$ (Reprinted with permission from Recher et al. [68]. Copyright (2009) by the American Physical Society)

2. The linear dispersion in graphene implies that the electron velocity is a constant v_F rather than proportional to the momentum p/m. Therefore, the spin–orbit coupling in graphene is independent of p.
3. While GaAs is piezoelectric, graphene is not. Whereas the dominant electron–phonon coupling mechanism in GaAs is piezoelectric, the deformation potential dominates in graphene.
4. Because graphene is a two-dimensional solid, the acoustic phonon density of states is linear rather than quadratic in the phonon frequency (energy). Also, in a precisely flat and infinite 2D crystal, the out-of-plane lattice vibrations have a quadratic dispersion, leading to a diverging density of states at zero energy. Thus, the flexural phonons destabilize the graphene sheet, but in practice, this is prevented by the support on a substrate, the finite size of the sample, the tension from the support, the presence of frozen ripples, etc.

A calculation done for graphene, similar to the one described in Sec. V for GaAs QDs, yields a finite relaxation rate at zero magnetic field, if one assesses a perfectly flat and infinite graphene sample [70]. However, for realistic samples, one expects that the out-of-plane modes are gapped or at least assume a linear dispersion at small wave vectors which then implies a crossover to a $T_1 \propto B^{-2}$ behavior (Fig. 8) [70].

Hyperfine Interaction in Graphene

If the valley degeneracy is lifted, the electron spin decoherence in a graphene QD with lifted valley degeneracy due to the 1 % ^{13}C atoms can be calculated in a similar way as described in section "Nuclear-Spin-Induced Decoherence." [71]

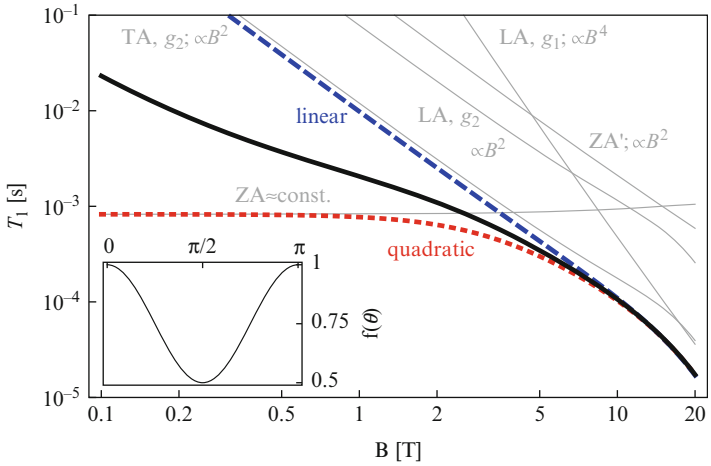

Fig. 8 Theoretically calculated spin relaxation time T_1 in a circular graphene quantum dot, as a function of the applied perpendicular magnetic field [70]. *Inset*: anisotropy, in dependence on the direction of the magnetic field (Reprinted with permission from Struck and Burkard [70]. Copyright (2010) by the American Physical Society)

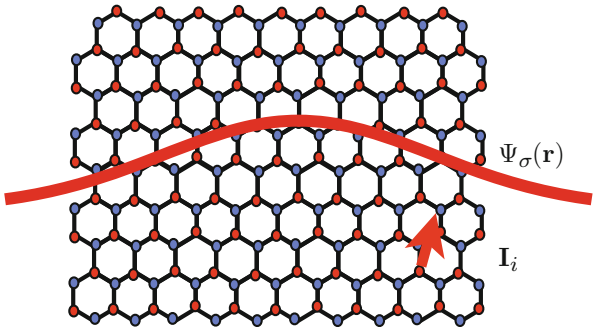

Fig. 9 In graphene, every one in one hundred carbon atoms is a ^{13}C atom with nuclear spin 1/2, while the remaining atoms are ^{12}C without nuclear spin. The ^{13}C atoms act as weak but strongly localized scatterers, thus allowing for large momentum scattering from one valley to the other

The differences between the hyperfine-induced decoherence in graphene and GaAs are (1) small abundance of nuclear-spin-carrying atoms in natural carbon and (2) the smallness and anisotropy of the hyperfine tensor. Regarding the latter, the hyperfine interaction in graphene is typically more than 100 times smaller in graphene than in III–V semiconductors, i.e., below 1 μeV. The atomic orbitals that form the relevant bands in graphene are carbon p orbitals (rather than s orbitals as in the GaAs conduction band), and the contact hyperfine interaction $\propto |\psi_p(\mathbf{R})|^2$ vanishes. The dipolar coupling leads to a somewhat smaller and anisotropic coupling [71]. In naturally occurring carbon, about 1 % of the carbon atoms in the graphene host material are ^{13}C atoms with nuclear spin I = 1/2, the rest being ^{12}C with spin $I = 0$. Starting from the hopping model for graphene and adding the hyperfine interaction term, one obtains at the low-energy Dirac Hamiltonian [72]

$$H_{\mathrm{hf}} \simeq \mathbf{S} \cdot \left(\mathbf{h}^{(0)} \tau_0 + \sum_{i=x,y,z} \mathbf{h}^{(i)} \tau_i \right), \tag{46}$$

with the ordinary hyperfine field $\mathbf{h}^{(0)}$ as in Eq. 36 for GaAs plus the valley-flip fields $\mathbf{h}^{(x)}$ and $\mathbf{h}^{(x)}$. The origin of the $\mathbf{h}^{(x)}$ and $\mathbf{h}^{(y)}$ terms lies in the following fact about the hyperfine coupling: The ^{13}C atoms give rise to a weak but very strongly localized impurity potential which is able to scatter electrons from one valley to the other (Fig. 9).

Conclusion

Electron and nuclear spins are promising building blocks for future quantum hardware. The search for suitable nuclear-spin-free materials and devices which allow for long spin coherence times has stimulated the research of graphene, carbon nanotubes, and silicon nanostructures and devices. Challenges for future research consist in the absence of a bandgap in graphene and the influence of the valley degeneracy present in all these material systems on the spin-related electronic properties, e.g., spin coherence and spin exchange coupling.

References

1. Struck PR (2013) Spin coherence in carbon-based nanodevices. Chapter 2, PhD thesis, University of Konstanz
2. Shor P (1994) Algorithms for quantum computation: discrete logarithms and factoring. Proceedings of the 35th annual symposium on the foundations of computer science. IEEE Press, Los Alamitos, p 124
3. DiVincenzo DP (2000) The physical implementation of quantum computation. Fortschr Phys 48:771; quant-ph/0002077
4. Nielsen MA, Chuang IL (2000) Quantum computation and quantum information. Cambridge University Press, Cambridge, UK
5. Preskill J (1998) Reliable quantum computers. Proc Roy Soc Lond A 454:385
6. Mermin ND (2007) Quantum computer science: an introduction. Cambridge University Press, Cambridge, UK
7. Knill E (2005) Quantum computing with realistically noisy devices. Nature 434:39
8. Fowler AG, Mariantoni M, Martinis JM, Cleland AN (2012) Surface codes: Towards practical large-scale quantum computation. Phys Rev A 86:032324
9. DiVincenzo DP (1995) Two-qubit gates are universal for quantum computation. Phys Rev A 51:1015
10. Barenco A et al (1995) Elementary gates for quantum computation. Phys Rev A 52:3457
11. Loss D, DiVincenzo DP (1998) Quantum computation with quantum dots. Phys Rev B 57:120
12. Cirac JI, Zoller P (2012) Goals and opportunities in quantum simulation. Nat Phys 8:264
13. Deutsch D (1985) Quantum theory, the Church-Turing principle and the universal quantum computer. Proc Roy Soc Lond A 400:97
14. Kane BE (1998) A silicon-based nuclear spin quantum computer. Nature 393:6681
15. Vrijen R, Yablonovitch E, Wang K, Jiang HW, Balandin A, Roychowdhury V, Mor T, DiVincenzo DP (2000) Electron-spin-resonance transistors for quantum computing in silicon-germanium heterostructures. Phys Rev A 62:012306

16. Barnes CHW, Shilton JM, Robinson AM (2000) Quantum computation using electrons trapped by surface acoustic waves. Phys Rev B 62:8410
17. Kloeffel C, Loss D (2013) Prospects for Spin-based quantum computing. Annu Rev Condens Matter Phys 4:51; arXiv:1204.5917
18. Hanson R, Kouwenhoven LP, Petta JR, Tarucha JR, Vandersypen LMK (2007) Spins in few-electron quantum dots. Rev Mod Phys 79:1217
19. Burkard G, Loss D, DiVincenzo D (1999) Coupled quantum dots as quantum gates. Phys Rev A 59:2070
20. Petta JR et al (2005) Coherent Manipulation of Coupled Electron Spins in Semiconductor Quantum Dots. Science 309:2180
21. Kavokin KV (2001) Anisotropic exchange interaction of localized conduction-band electrons in semiconductors. Phys Rev B 64:075305
22. Bonesteel NE, Stepanenko D, DiVincenzo DP (2001) Anisotropic spin exchange in pulsed quantum gates. Phys Rev Lett 87:207901
23. Koppens FHL et al (2006) Driven coherent oscillations of a single electron spin in a quantum dot. Nature 442:766
24. Brunner R et al (2011) Two-qubit gate of combined single-spin rotation and interdot spin exchange in a double quantum dot. Phys Rev Lett 107:146801
25. DiVincenzo DP, Bacon D, Kempe J, Burkard G, Whaley KB (2000) Universal quantum computation with the exchange interaction. Nature 408:339
26. Kawano Y et al (2005) Existence of the exact CNOT on a quantum computer with the exchange interaction. Quantum Inf Process 4:65
27. Fong BH, Wandzura SM (2011) Universal quantum computation and leakage reduction in the 3-qubit decoherence free subsystem. J Quantum Inf Comput 11:1003; arXiv:quant-ph/0411013
28. Zeuch D (2011) Quantum computation with restricted spin interactions. Diploma thesis, University of Konstanz
29. Medford J et al (2013) Quantum-dot-based resonant exchange qubit. Phys Rev Lett 111:050501
30. Taylor JM, Srinivasa V, Medford J (2013) Electrically protected resonant exchange qubits in triple quantum dots. Phys Rev Lett 111:050502
31. Doherty AC, Wardrop MP (2013) Two-qubit gates for resonant exchange qubits. Phys Rev Lett 111:050503
32. Levy J (2002) Universal quantum computation with spin-1/2 pairs and Heisenberg exchange. Phys Rev Lett 89:147902
33. Kempe J, Whaley KB (2002) Exact gate sequences for universal quantum computation using the XY interaction alone. Phys Rev A 65:052330
34. Vala J, Whaley KB (2002) Encoded universality for generalized anisotropic exchange hamiltonians. Phys Rev A 66:022304
35. Burkard G, Loss D, DiVincenzo DP, Smolin JA (1999) Physical optimization of quantum error correction circuits. Phys Rev B 60:11404
36. Khaetskii AV, Nazarov YV (2001) Spin-flip transitions between zeeman sublevels in semiconductor quantum dots. Phys Rev B 64:125316
37. Dyakonov MI, Yu V (1986) Spin relaxation of two-dimensional electrons in noncentrosymmetric semiconductors. Kachorovskii Fiz Tech Poluprovodn 20:178; Sov Phys Semicond 20:110
38. van Vleck J (1940) Paramagnetic relaxation times for titanium and chrome alum. Phys Rev 57:426
39. Amasha S, MacLean K, Radu IP, Zumbühl DM, Kastner MA, Hanson MP, Gossard AC (2008) Electrical control of spin relaxation in a quantum dot. Phys Rev Lett 100:46803
40. Bulaev DV, Loss D (2005) Spin relaxation and decoherence of holes in quantum dots. Phys Rev Lett 95:076805
41. Heiss D et al (2007) Observation of extremely slow hole spin relaxation in self-assembled quantum dots. Phys Rev B 76:241306

42. Gerardot BD et al (2008) Optical pumping of a single hole spin in a quantum dot. Nature 451:441
43. Golovach VN, Khaetskii AV, Loss D (2004) Phonon-induced decay of the electron spin in quantum dots. Phys Rev Lett 93:016601
44. Coish WA (2006) Spins in quantum dots: Hyperfine interaction, transport, and coherent control. PhD thesis, University of Basel
45. Coish WA, Baugh J (2009) Nuclear spins in nanostructures. Phys Status Solidi B 246:2203
46. Urbaszek B et al (2013) Nuclear spin physics in quantum dots: An optical investigation. Rev Mod Phys 85:79
47. Klauser D, Coish WA, Loss D (2006) Nuclear spin state narrowing via gate-controlled Rabi oscillations in a double quantum dot. Phys Rev B 73:205302
48. Fischer J, Coish W, Bulaev D, Loss D (2008) Spin decoherence of a heavy hole coupled to nuclear spins in a quantum dot. Phys Rev B 78:155329
49. Coish WA, Loss D (2004) Hyperfine interaction in a quantum dot: Non-Markovian electron spin dynamics. Phys Rev B 70:195340
50. Chekhovich EA et al (2010) Pumping of nuclear spins by optical excitation of spin-forbidden transitions in a quantum dot. Phys Rev Lett 104:066804
51. Foletti S, Bluhm H, Mahalu D, Umansky V, Yacoby A (2009) Universal quantum control of two-electron spin quantum bits using dynamic nuclear polarization. Nat Phys 5:903
52. Ribeiro H, Burkard G (2009) Nuclear state preparation via landau-zener-stückelberg transitions in double quantum dots. Phys Rev Lett 102:216802
53. Stepanenko D, Burkard G, Giedke G, Imamoglu A (2006) Enhancement of electron spin coherence by optical preparation of nuclear spins. Phys Rev Lett 96:136401
54. Togan E, Chu Y, Imamoglu A, Lukin MD (2011) Laser cooling and real-time measurement of the nuclear spin environment of a solid-state qubit. Nature 478:497501
55. Taylor JM et al (2005) Fault-tolerant architecture for quantum computation using electrically controlled semiconductor spins. Nat Phys 1:177
56. Hanson R, Burkard G (2007) Universal set of quantum gates for double-dot spin qubits with fixed interdot coupling. Phys Rev Lett 98:050502
57. Trauzettel B, Bulaev DV, Loss D, Burkard G (2007) Spin qubits in graphene quantum dots. Nat Phys 3:192
58. Diez M, Burkard G (2012) Bias-dependent D'yakonov-Perel'spin relaxation in bilayer graphene. Phys Rev B 85:195412
59. Kormanyos A et al (2013) Intrinsic and substrate induced spin-orbit interaction in chirally stacked trilayer graphene. Phys Rev B 88:045416
60. Klinovaja J, Loss D (2013) Spintronics in MoS_2 monolayer quantum wires. Phys Rev B 88:075404
61. Rohling N, Burkard G (2012) Universal quantum computing with spin and valley states. New J Phys 14:083008
62. Katsnelson MI (2012) Graphene: Carbon in Two Dimensions. Graphene. Cambridge University Press
63. Brey L, Fertig HA (2006) Electronic states of graphene nanoribbons studied with the Dirac equation. Phys Rev B 73:235411
64. Tworzydło J, Trauzettel B, Titov M, Rycerz A, Beenakker CWJ (2006) Sub-poissonian shot noise in graphene. Phys Rev Lett 96:246802
65. Liu XL, Hug D, Vandersypen LMK (2010) Gate-defined graphene double quantum dot and excited state spectroscopy. Nano Lett 10:1623
66. Braun M, Struck PR, Burkard G (2011) Spin exchange interaction with tunable range between graphene quantum dots. Phys Rev B 84:115445
67. Giovannetti G, Khomyakov PA, Brocks G, Kelly PJ, van den Brink J (2007) Substrate-induced band gap in graphene on hexagonal boron nitride: *Ab initio* density functional calculations. Phys Rev B 76:073103

68. Recher P, Nilsson J, Burkard G, Trauzettel B (2009) Bound states and magnetic field induced valley splitting in gate-tunable graphene quantum dots. Phys Rev B 79:85407
69. Goossens ASM et al (2012) Gate-defined confinement in bilayer graphene-hexagonal boron nitride hybrid devices. Nano Lett 12:4656
70. Struck PR, Burkard G (2010) Effective time-reversal symmetry breaking in the spin relaxation in a graphene quantum dot. Phys Rev B 82:125401
71. Fischer J, Trauzettel B, Loss D (2009) Hyperfine interaction and electron-spin decoherence in graphene and carbon nanotube quantum dots. Phys Rev B 80:155401
72. Palyi A, Burkard G (2009) Hyperfine-induced valley mixing and the spin-valley blockade in carbon-based. Phys Rev B 80:201404(R)